Published in final edited form as:
Biochemistry. 2013 May 21; 52(20): . doi:10.1021/bi400230u.

Analysis of SNARE complex/Synaptotagmin-1 Interactions by One-dimensional NMR Spectroscopy†

Amy Zhou, **Kyle D. Brewer**, and **Josep Rizo***
Departments of Biophysics, Biochemistry and Pharmacology, University of Texas Southwestern Medical Center, 6000 Harry Hines Boulevard, Dallas, Texas 75390, USA

Abstract

Neurotransmitter release depends critically on the Ca^{2+} sensor synaptotagmin-1 and the SNARE proteins syntaxin-1, synaptobrevin and SNAP-25, which mediate membrane fusion by forming tight SNARE complexes that bridge the synaptic vesicle and plasma membranes. Interactions between the SNARE complex and the two C_2 domains of synaptotagmin-1 (the C_2A and C_2B domains) are believed to play a key role in coupling Ca^{2+} sensing to membrane fusion, but the nature of these interactions is unclear, in part because of a paucity of data obtained by quantitative biophysical methods. Here we have analyzed synaptotagmin-1/SNARE complex interactions by monitoring the decrease in the intensities of one-dimensional ^{13}C-edited ^{1}H-NMR spectra of ^{13}C-labeled fragments of synaptotagmin-1 upon binding to unlabeled SNARE complex. Our results indicate that there is a primary binding mode between synaptotagmin-1 and the SNARE complex that involves a polybasic region in the C_2B domain and has a submicromolar affinity. Our NMR data, combined with precipitation assays, show that there are additional SNARE complex/synaptotagmin-1 interactions that lead to aggregation and that involve in part two arginines at the bottom of the C_2B domain. Overall, this study shows the importance of disentangling the contributions of different types of interactions to SNARE complex/synaptotagmin-1 binding, and illustrate the usefulness of one-dimensional NMR methods to analyze intricate protein interactions.

Introduction

The release of neurotransmitters by Ca^{2+}-evoked synaptic vesicle exocytosis is an exquisitely regulated process that is key for communication between neurons. Crucial components of the complex protein machinery that controls release are the synaptic vesicle protein synaptotagmin-1 and the soluble N-ethylmaleimide sensitive factor attachment protein receptor (SNARE)[1] proteins synaptobrevin, syntaxin-1 and SNAP-25 [reviewed in (1–4)], which mediate Ca^{2+}-triggered membrane fusion in a tight interplay with other key proteins (5). The three SNAREs form a four-helix bundle called the SNARE complex through their SNARE motifs (two from SNAP-25 and one each from synaptobrevin and syntaxin-1) (6;7). Assembly of the SNARE complex brings the synaptic vesicle and plasma membranes together (8), which is critical for membrane fusion. Synaptotagmin-1 contains two C_2 domains (the C_2A and C_2B domains) that form most of its cytoplasmic region and adopt β-sandwich structures, binding three or two Ca^{2+} ions, respectively, through loops at the top of the sandwich (9–12) (Figure 1). These top loops also mediate Ca^{2+}-dependent binding of synaptotagmin-1 to phospholipids (12–14). Point mutations that impair or

†This work was supported by grant I-1304 from the Welch Foundation and grant NS404944 from the National Institutes of Health (to J.R.). K.D.B. was supported in part by training grant T32 GM008297 from the National Institutes of Health.

*To whom correspondence should be addressed. Telephone: 214-645-6361. FAX: 214-645-6291. jose@arnie.swmed.edu.

enhance this activity lead to parallel effects on the efficiency of neurotransmitter release (15;16), demonstrating that synaptotagmin-1 is the major Ca^{2+} sensor for fast neurotransmitter release and showing the functional importance of Ca^{2+}-dependent phospholipid binding to synaptotagmin-1.

Ca^{2+} binding to the C_2B domain is particularly crucial for synaptotagmin-1 function (17–20), which may arise in part from its contribution to Ca^{2+}-dependent phospholipid binding (21) and/or from its ability to bind simultaneously to two apposed membranes through the top loops and through two arginine side chains (R398 and R399) at the bottom of the domain (22) (Figure 1). Indeed, mutation of these two arginines almost completely abolishes neurotransmitter release and strongly impairs the ability of synaptotagmin-1 to cluster liposomes as well as to stimulate SNARE-dependent lipid mixing between liposomes (23). In addition, the C_2B domain contains a polybasic region on the side of the β-sandwich (Figure 1) that was also implicated in binding to negatively charged phospholipids, including phosphoinositides (24), and mutations in this region also cause considerable (albeit more moderate) impairments in neurotransmitter release (25;26).

Synaptotagmin-1 function is widely believed to also depend on interactions with the SNAREs, which could provide a natural means to couple Ca^{2+} sensing to membrane fusion. However, it has been difficult to pinpoint how synaptotagmin-1/SNARE interactions mediate this coupling, in part because multiple types of such interactions were described. Initial work reported interactions between synaptotagmin-1 and syntaxin-1 that were Ca^{2+}-dependent or Ca^{2+}-independent, involved the C_2A domain, the C_2B domain, or both, and were ascribed to the syntaxin-1 SNARE motif or its N-terminal H_{abc} domain (27–33). Later work also revealed binding of synaptotagmin-1 to SNAP-25, to syntaxin-1/SNAP-25 heterodimers and to the SNARE complex that again was Ca^{2+}-dependent or Ca^{2+}-independent, and ascribed preponderant roles to the synaptotagmin-1 C_2A domain, the C_2B domain or both, depending on the study (34–42). Several of the interactions that have been described probably arose from the promiscuity of these proteins (43) and hence may not physiologically relevant. However, interactions involving the SNARE complex are generally believed to play a role in neurotransmitter release because synaptotagmin-1 action occurs in the late steps of Ca^{2+}-evoked exocytosis, when the SNARE complex is expected to be at least partially assembled. In fact, these interactions are likely key to couple Ca^{2+} sensing to membrane fusion but, unfortunately, they are still poorly understood. Thus, SNARE complex/synaptotagmin-1 binding was proposed to involve an acidic region in the middle of the SNAP-25 N-terminal SNARE motif (44) or an acidic region at the C-terminal half of the SNAP-25 C-terminal SNARE motif (36;41). Moreover, while some data suggest that binding involves the polybasic region of the C_2B domain but not the two arginines at the bottom (23;41;44), other results suggested that both regions are involved (45), and a model built from single-molecule fluorescence spectroscopy data places the SNARE complex closest to the helix at the bottom of the C_2B domain (46).

Some of the discrepancies between different studies might be due to the highly charged nature of synaptotagmin-1 and the SNARE complex, which may underlie binding in different modes, but inconsistencies may have also arisen from the frequent use of biochemical methods that, while powerful for initial exploratory studies, are prone to artifacts and/or are not adequate to obtain reliable quantitative data [see (47)]. In order to understand how SNARE complex/synaptotagmin-1 interactions control neurotransmitter release, it is critical to determine whether one major binding mode exists, what is the stoichiometry of binding, and how much non-specific interactions contribute to overall binding. For this purpose, it is necessary to use quantitative analytical methods that can define the relative contributions of different binding modes, as well as the effects of point mutations on binding. Unfortunately, these studies are hindered by the high tendency of

SNARE complex/synaptotagmin-1 assemblies to precipitate in the presence of Ca^{2+} even at protein concentrations on the 10 μM range [(41); see also below].

In the research described here, we have explored the use of one-dimensional (1D) ^{13}C-edited ^{1}H-NMR spectroscopy (48) to analyze SNARE complex/synaptotagmin-1 interactions in solution quantitatively. Our results show that SNARE complex binding in solution is dominated by the synaptotagmin-1 C_2B domain. Moreover, our data indicate that the polybasic region of the C_2B domain constitutes the primary binding site for the SNARE complex, whereas the two arginines at the bottom of the C_2B domain mediate additional, weaker interactions that lead to aggregation and precipitation of SNARE complex/synaptotagmin-1 assemblies. Overall, this study emphasizes the complexity of analyzing SNARE complex/synaptotagmin-1 interactions and illustrates the usefulness of 1D NMR methods to study protein complexes.

EXPERIMENTAL PROCEDURES

Protein Expression and Purification

Constructs for expression of rat synaptotagmin-1 C_2A domain (residues 140–267), C_2B domain (residues 271–421) and C_2AB fragment (residues 140– 421), as well as the SNARE motifs of rat synaptobrevin (residues 29–93), rat syntaxin-1A (residues 191–253), and human SNAP-25B (residues 11–82 and 141–203) were previously described (9;22;49;50). Mutations were performed using the QuickChange site-directed mutagenesis kit (Stratagene). All proteins were expressed as GST-fusions in *Escherichia coli* BL21(DE3) cells. Unlabeled proteins were expressed in LB broth, while uniform ^{13}C- and ^{15}N-labeling was achieved through expression in M9 minimal media with $^{13}C_6$ -glucose as the sole carbon source and $^{15}NH_4Cl$ as the sole nitrogen source.

SNARE proteins were purified by affinity chromatography, followed by ion exchange and/or gel filtration as described (50). For synaptotagmin-1 fragments, the cell pellet was resuspended in cold Lysis Buffer (40 mM Tris-HCl pH 8.2, 200 mM NaCl, 2 mM DTT) with 1% Triton and protease inhibitors (1 mM each of Sigma Inhibitor cocktail, ABESF, EGTA, and EDTA). The suspension was frozen in liquid nitrogen and thawed at RT. The cells were passed four times through an EmulsiFlex-C5 cell homogenizer (Avestin) at 13,000 psi, spun at 19000 rpm for 30 minutes, and incubated for one hour at RT with 100 mg protamine sulfate (Sigma-Aldrich) per 35 ml supernatant. The mixture was spun again at 19000 rpm for 30 minutes, and the supernatant was passed through a 0.8 μm syringe filter before mixing with prewashed Glutathione Sepharose 4B beads (GE Healthcare) at a ratio of 1 ml of bead slurry per 1 L culture. Incubation was either three hours at RT or overnight at 4°C. The resin was extensively washed with 200 ml each of the following buffers: Lysis Buffer, Lysis Buffer with 50 mM $CaCl_2$, and Lysis Buffer with 50 mM $CaCl_2$ and 1 M NaCl. The resin was then equilibrated with Benzonase buffer (50 mM Tris-HCl, pH 8.0, 2 mM $MgCl_2$, 2 mM DTT) before the addition of 20 ml Benzonase buffer and 5 μl Benzonase Nuclease (Novagen, 25 KUN) and rotation at RT for 3 hours. The Benzonase wash was discarded and the resin was extensively washed with high ionic strength buffer (1 M NaCl in benzonase buffer or TCB – see below). The resin was then equilibrated with Thrombin Cleavage buffer (TCB: 50 mM Tris-HCl, pH 8.0, 150 mM NaCl, 2.5 mM $CaCl_2$, 2 mM DTT). Thrombin cleavage was carried out at RT for 3 hrs or at 4°C overnight in 10 ml TCB and 0.08 mg/ml thrombin (Sigma-Aldrich). The cleavage fraction was collected and elution was repeated with TCB until UV Abs_{280} was < 0.1 to recover the maximal amount of protein from the resin.

For the WT and mutant C_2AB fragment, the elution fractions were combined and diluted with buffer A (50 mM NaAc pH 6.2, 5 mM $CaCl_2$) so that [NaCl] ≤ 100 mM. Cation-

exchange on a Source S column (GE Life Sciences) was performed in buffer A with a linear gradient from 0.1 to 0.7 M NaCl in 30 column volumes. This was followed by gel filtration on Superdex 75 (25 mM HEPES-NaOH pH 7.4, 125 mM NaCl). For the WT and mutant C_2B domain, the elution fractions were concentrated after adding 2.5 mM EDTA, and samples were purified on a Superdex 75 column in gel filtration buffer (0.2 M phosphate, pH 6.3, 0.3 M NaCl). The gel filtration elution was buffer-exchanged using a 10 kDa centrifugal filter unit into 20 mM MES pH 6.3, and was then loaded onto a SourceS column where cation-exchange was carried out in 20 mM MES, pH 6.3, 20 mM $CaCl_2$ using a linear gradient from 0.1 to 0.6 M NaCl in 40 column volumes. At least two distinct peaks normally emerged, both corresponding to protein of the correct molecular weight. Only the later fractions contain C_2B domain devoid of acidic contaminants. These fractions were collected and buffer exchanged to the same final buffer into 25 mM HEPES-NaOH pH 7.4, 125 mM NaCl. For both the C_2AB fragment and the C_2B domain, 0.3 mM TCEP and 1 mM ABESF were added to the final purified proteins, but EDTA and EDTA-containing inhibitor cocktails were avoided.

Proper folding of the synaptotagmin-1 C_2AB fragment mutants was confirmed through their ^1H-^{15}N TROSY-HSQC spectra. The SNARE motifs of synaptobrevin, syntaxin-1 and SNAP-25 were mixed in equimolar ratio and incubated overnight at 4°C to assemble the SNARE complex. Isolated SNARE motifs that did not incorporate into SNARE complexes were removed by extensive concentration-dilution in a 10 kDa Amicon centrifugal filter (50). The purity of the final SDS-resistant complex was verified SDS-PAGE and Coomassie blue staining.

NMR Spectroscopy

All NMR spectra were acquired at 25°C on Varian INOVA 500MHz or 600MHz spectrometers. Samples were prepared in 25 mM HEPES (pH 7.4) and 125 mM NaCl with 5% D_2O. Standard conditions for titrations assays included 1 mM Ca^{2+} unless otherwise indicated. For Ca^{2+}-free samples, 1 mM EDTA was added. 1D ^{13}C-edited ^1H-NMR spectra were obtained by acquiring the first trace of a ^1H-^{13}C heteronuclear single quantum coherence spectrum as previously described (48). Total acquisition times were 20–40 min for spectra acquired on cold probes and 1 hr for spectra acquired on room temperature probes. Spectra were analyzed with the VnmrJ software (Agilent Technologies Inc., Santa Clara, CA).

Titrations with SNARE complex

Samples contained a constant amount of uniformly ^{15}N,^{13}C-labeled C_2AB fragment (2.4–3 μM) and the indicated concentrations of unlabeled SNARE complex. A new sample was prepared for each titration point, rather than adding SNARE complex to the same sample. For each point of the titration, we subtracted a 1D ^{13}C-edited ^1H-NMR spectrum of a sample containing 20 μM unlabeled SNARE complex scaled according to the concentration of SNARE complex corresponding to that point of the titration in order to account for the 1% natural abundance of ^{13}C isotope. Assuming a 1:1 equilibrium-binding model where the C_2AB fragment is considered as the protein and the SNARE complex as the ligand, the strongest methyl resonance (SMR) intensity resulting after the subtraction (I) can be expressed as a function of L_T, the total SNARE complex concentration added by equation (1):

$$I = I_f + (I_b - I_f)\frac{P_T + L_T + K_d - \sqrt{(P_T + L_T + K_d)^2 - 4P_T L_T}}{2P_T} \quad (1)$$

where I_f represents the SMR intensity of the free $^{15}N,^{13}C$-labeled C_2AB fragment, I_b is the SMR intensity of the $^{15}N,^{13}C$-labeled C_2AB fragment bound to the SNARE complex, P_T is the total concentration of $^{15}N,^{13}C$-labeled C_2AB fragment, and K_d is the dissociation constant. The experimental data were fit to this equation using Sigma Plot (Systat Software Inc.) to derive the I_f, I_b and K_d parameters. After an initial fit, the calculated value of I_f was then used to normalize all the intensities, which allows comparison between data sets obtained at different times and different instruments. Hence, the value of I_f after the normalization is 1 and the I_b values are expressed as a fraction of I_f. The values of I_b and K_d described below and their errors were obtained by fitting separate data sets and then calculating the average and standard deviations of the I_b and K_d values obtained (2 to 4 data sets for each condition).

Synaptotagmin-1 fragment/SNARE complex precipitation assays

Samples containing 10 μM WT or mutant synaptotagmin-1 C2AB fragment or C2B domain were mixed with 10 or 20 μM SNARE complex under the same conditions as the NMR experiments (25 mM HEPES-NaOH, 125 mM NaCl, 1 mM Ca^{2+}, pH 7.4). The total reaction volume was 50 μl. After 5 min incubation at room temperature, the samples were centrifuged at 13,000 rpm for 1.5 minutes in a benchtop centrifuge (Eppendorf AG 5415 D), and the supernatant was separated from the pellet. The pellet was resuspended in 50 μl buffer, and 5 μl of each of the supernatant and pellet fractions were analyzed by SDS PAGE using 15% polyacrylamide gels in Tris-Glycine-SDS running buffer, followed by Coomassie blue staining.

RESULTS

Ca^{2+}enhancement of SNARE complex/synaptotagmin-1 binding

Over the years we have made many attempts to analyze interactions between a synaptotagmin-1 fragment spanning its two C_2 domains (residues 140–421; referred to as the C_2AB fragment) and a minimal SNARE complex formed by the SNARE motifs of synaptobrevin, syntaxin-1 and SNAP-25 (below referred to as the SNARE complex for simplicity). As mentioned above, these studies were hampered by the high tendency of SNARE complex/synaptotagmin-1 assemblies to aggregate in the presence of Ca^{2+} [(41); see also below]. Note in this context that the C_2AB fragment as well as the individual C_2A and C_2B domains are highly soluble at physiological conditions in the absence and presence of Ca^{2+}, remaining monomeric even at concentrations close to 1 mM (12;22;31;49;51), and that the SNARE complex that we use lacks a few residues at the C-terminus of syntaxin-1 to enhance its solubility, remaining monomeric at concentrations well above 100 μM (50;52). Thus, the insolubility of SNARE complex/C_2AB fragment assemblies likely arises from charge neutralization, as the SNARE complex is highly acidic and the C_2AB fragment contains abundant basic regions (particularly the C_2B domain). During our studies we found that precipitation in the presence of 1 mM Ca^{2+} at physiological pH and ionic strength was largely avoided if the concentration of either the C_2AB fragment or the SNARE complex was kept at 3 μM or below. Because of this constraint and because of the low enthalpies of SNARE complex/synaptotagmin-1 interactions, we were unable to obtain reliable quantitative data on these interactions by isothermal titration calorimetry (ITC). Thus, we explored the use of a method that relies on 1D ^{13}C-edited 1H-NMR spectroscopy and that we developed as an alternative to ITC to study protein interactions quantitatively (48).

The method is based on measuring the intensity of the strongest methyl resonance (SMR) in 1D ^{13}C-edited 1H-NMR spectra of a ^{13}C-labeled protein, and quantifying the decrease in the SMR intensity upon binding to an unlabeled protein or macromolecule due to the resulting increase in the rotational correlation time and the corresponding resonance broadening. This

method can be used with high sensitivity at low micromolar protein concentrations (even without a cryo-probe) because the methyl signals are not spread in additional dimensions as is common in multidimensional NMR experiments. As shown below, qualitative analysis of additional methyl resonances that are still observable at these low protein concentrations provides additional information to interpret the binding experiments. Although ^{15}N-labeling is not necessary to acquire 1D ^{13}C-edited 1H-NMR spectra, we used ^{15}N,^{13}C-labeled synaptotagmin-1 fragments in our experiments to allow verification of the purity of the fragments using 1H-^{15}N HSQC spectra [(49), see also below]. Since SNARE complex/synaptotagmin-1 interactions are highly sensitive to the ionic strength (40), all experiments described in this study were performed with a constant ionic strength that resembles physiological conditions.

We first acquired 1D ^{13}C-edited 1H-NMR spectra of 3 μM ^{15}N,^{13}C-labeled C_2AB fragment in the absence and presence of a small excess (3.5 μM) of unlabeled SNARE complex. We observed that the SNARE complex induced a small decrease in SMR intensity when 1 mM EDTA was present (Figure 2A), indicating weak binding. However, a much stronger decrease in SMR intensity was observed in parallel experiments performed in the presence of 1 mM Ca^{2+} (Figure 2A). Since Ca^{2+} itself did not significantly affect the SMR intensity of the C_2AB fragment, these results showed that, as expected, Ca^{2+} strongly enhances binding of the C_2AB fragment to the SNARE complex. Ca^{2+} titrations in the presence of 3.5 μM SNARE complex revealed a progressive decrease in SMR intensity that saturates at about 300 μM Ca^{2+} (e.g. Figures 2B,C). Fitting of three independent experiments to a Hill equation yielded an average value of 58 ± 8 μM for the microscopic dissociation constant, and an average Hill coefficient of 1.2±0.3 (all errors are given as standard deviations). These results suggest that there is almost no cooperativity among the C_2 domain Ca^{2+}-binding sites in enhancing SNARE complex binding, as expected from the absence of cooperativity in intrinsic Ca^{2+} binding to the five sites of the synaptotagmin-1 C_2 domains (10;12) if the SNARE complex does not contribute directly to coordinate the Ca^{2+} ions. However, the observed microscopic dissociation constant is considerably lower that the intrinsic dissociation constants of the individual Ca^{2+} binding sites of the C_2B domain [300–600 μM; see (12)]. Because SNARE complex binding involves primarily the C_2B domain (see below), these observations suggest that there is some cooperativity between Ca^{2+} binding and SNARE complex binding to the C_2AB fragment. Such cooperativity may arise from long-range electrostatic interactions, as the SNARE complex is strongly negatively charged (7) and Ca^{2+}-binding increases the positive charge of the C_2 domains (12;31).

Mutational analysis of SNARE complex/synaptotagmin-1 C_2AB fragment interactions

To study the affinity of the C_2AB fragment for the SNARE complex, we performed titrations of ^{15}N, ^{13}Clabeled C_2AB fragment with increasing amounts of unlabeled SNARE complex monitored with 1D ^{13}C-edited 1H-NMR spectra. In the presence of 1 mM EDTA, we observed only modest decreases in the SMR intensity that were far from saturation at 40 μM SNARE complex and hence did not allow reliable measurement of the dissociation constant. However, titrations of ^{15}N,^{13}C-labeled C_2AB fragment with unlabeled SNARE complex in the presence of 1 mM Ca^{2+} led to much stronger decreases in SMR intensity that appeared to be saturable at least to some degree (e.g. Figure 3A). To make the results obtained with different samples on different days or instruments comparable, all the data were normalized to the intensity at zero SNARE complex concentration (I_f). For this purpose, we first fitted each data set with the absolute intensities measured and obtained an intensity at zero SNARE complex concentration that was then used to normalize the data set. Curve fitting of multiple titrations assuming a standard protein to ligand binding model with a 1:1 stoichiometry (Equation 1) yielded an apparent K_d of 2.32 ± 0.15 μM (Table 1).

We next investigated how SNARE complex/C_2AB fragment binding as reported by 1D ^{13}C-edited 1H-NMR spectra is affected by mutations that had previously been described to impair binding based on other analytical methods, in some cases with contradictory results. These mutations included: i) a D232N substitution in the C_2A domain (referred to as DN mutation) that abolishes Ca^{2+} binding to two of its three Ca^{2+}-binding sites (10) and was described to enhance neurotransmitter release as well as SNARE complex binding (53); ii) an R398Q,R399Q mutation at the bottom of the C_2B domain (referred to as RR mutation) that abolishes neurotransmitter release (23) and was reported to impair SNARE binding in one study (45) but not another (23); and iii) a Lys326A,Lys327A mutation in the polybasic region of the C_2B domain (referred to as KK mutation) that impairs neurotransmitter release (25;26) and was found to decrease binding to the SNARE complex (41;44) and to inositide polyphosphates (24;26).

Titrations of the ^{15}N,^{13}C-labeled C_2AB fragment mutants with unlabeled SNARE complex (e.g. Figures 3B–D) yielded the following apparent K_d values: 0.73 ± 0.33 μM for the DN mutant, 0.94 ± 0.01 μM for the RR mutant, and 3.74 ± 1.29 μM for the KK mutant (Table 1). In principle, these results might suggest that the DN and RR mutations both increase the affinity of the C_2AB fragment for the SNARE complex, while the KK mutation decreases binding. However, comparison of the titrations performed with the WT C_2AB fragment with those performed with the DN and RR mutants (e.g. Figures 3B,C) showed that the fitted curves were undistinguishable for low SNARE complex concentrations (below 5 μM) and diverged at the higher concentrations. Hence, it became apparent from these comparisons that the differences in K_d values measured for the WT C_2AB fragment and these two mutants arise from the differences yielded by the fitting algorithm for I_b, which is the normalized signal intensity extrapolated at infinite SNARE complex concentration. Thus, the I_b values obtained in the titrations were 0.29 ± 0.07 for the WT C_2AB fragment, 0.44 ± 0.01 for the DN mutant, and 0.48 ± 0.03 for the RR mutant (Table 1). Assuming a 1:1 binding mode, which underlies equation 1, I_b is not expected to be altered by the mutations because it represents the normalized signal intensity corresponding to C_2AB fragment fully bound to the SNARE complex. These observations suggest that the intensity values observed during the titrations at low SNARE complex concentrations for the WT C_2AB fragment, as well as for the DN and RR mutants, reflect a primary, high affinity-binding mode that is not significantly affected by the DN and RR mutations. In addition, there appears to be one (or multiple) additional binding mode that is populated at higher SNARE complex concentrations and is impaired by the DN and RR mutations.

Further insights into this issue were obtained from comparison of the methyl region from 1D ^{13}C-edited ^{1}H-NMR spectra acquired without SNARE complex and with high SNARE complex concentrations (e.g. those in Figure 4). The SMR of the C_2AB fragment includes a group of overlapped resonances that is centered around ca. 0.87 ppm, and we estimate that the overall intensity of the SMR depends on the individual intensities of resonances with maxima ranging from 0.81 to 0.93 ppm. Based on the assignments obtained for the synaptotagmin-1 C_2A and C_2B domains (12;54), this region includes approximately 48 methyl resonances. Among these resonances, 7 of them (15%) correspond to methyl groups that have high mobility because they are in flexible regions. Because the molecular weights of the C_2AB fragment and the SNARE complex are 35 and 32 kDa, respectively, and because the SNARE complex is very elongated, formation of a 1:1 macromolecular assembly between them is expected to yield considerable broadening of the resonances from methyl groups in structured regions of the C_2AB fragment, while resonances from methyl groups that remain highly mobile upon binding should be much less affected. Nevertheless, based on our experience in NMR analyses of the SNARE complex [e.g. (41;50;52)], resonances containing contributions from multiple methyl groups in structured regions (e.g. between 0.4 and 0.6 ppm) should still be detectable upon binding of ^{15}N,^{13}C-C_2AB

fragment to the SNARE complex with 1:1 stoichiometry. This is indeed what we observed for the C_2AB fragment RR mutant at saturating SNARE complex concentrations (Figure 4B), suggesting that the results obtained for this mutant reflect 1:1 binding to the SNARE complex. However, only a sharp signal is observed at the position of the SMR for the WT C_2AB fragment (3 μM) in the presence of 20 μM SNARE complex, with no detectable resonances at lower chemical shifts (Figure 4B).

These observations indicate that the additional binding mode(s) occurring for the WT C_2AB at high SNARE complex concentrations involve the formation of large complexes and that the residual signal observed at the SMR position under these conditions corresponds to highly mobile methyl groups that are observable regardless of the molecular weight. This interpretation is further supported by the tendency of the WT C_2AB fragment to precipitate with the SNARE complex when both are at concentrations in the 10 μM range (see below). Hence, the apparent K_d measured in the titrations performed with the WT C_2AB fragment should not be considered reliable, and the corresponding I_b value does not correspond to 1:1 binding stoichiometry. Because the RR mutation disrupts, at least in part, formation of the larger complexes, the K_d measured for the RR mutant C_2AB fragment (0.94 μM) can be considered a better estimate of the dissociation constant for the primary SNARE complex/C_2AB fragment binding site, and 1:1 binding likely leads to an I_b value equal or larger to that measured for this mutant (0.48). Similar conclusions can be drawn for the DN mutant, although it appears that the DN mutation is less efficient at disrupting formation of large complexes than the RR mutation, as seen in the precipitation assays described below.

The I_b value obtained for the titrations performed with the KK mutant (0.34 ± 0.07, Table 1) was not significantly different from that obtained for the WT C_2AB fragment (0.29 ± 0.07), although we cannot rule out some perturbation of the secondary binding mode(s) by the KK mutation. Hence, the increased K_d measured for the KK mutant (3.74 ± 1.29 μM) cannot arise from differences in I_b values. Note also that the titrations performed with the KK mutant exhibited a clear divergence from those performed with the WT C_2AB fragment even at low SNARE concentrations (e.g. Figure 3D). Hence, these data show that the KK mutation impairs the primary binding mode between the C_2AB fragment and the SNARE complex. Nevertheless, it is clear that the complications in data analysis caused by the secondary binding mode(s) hinder the measurement of reliable K_ds and the quantification of the effects of mutations on the primary binding mode.

Contributions of the two synaptotagmin-1 C_2 domains to SNARE complex binding

Our analyses with the C_2AB fragment suggest that its primary binding site for the SNARE complex is located at the polybasic region of the C_2B domain. To further test this conclusion and to dissect the contributions of the two synaptotagmin-1 C_2 domains to SNARE complex, we performed titatrions of the isolated ^{15}N,^{13}C-labeled C_2A domain and C_2B domain with SNARE complex (Figure 5A). During these experiments it became apparent the importance of ensuring the purity of the isolated C_2B domain, which has a particularly high tendency to bind polyacidic compounds via the same polybasic region that binds to the SNARE complex (49). For optimal purification, we have modified slightly the protocol that we published previously (49), including a treatment with Benzonase nuclease (see Experimental Procedures). The purity of ^{15}N,^{13}C-C_2B domain samples obtained by this method was confirmed by the observation of a single set of cross-peaks in their ^{1}H-^{15}N HSQC spectra (e.g. Figure 5B, red contours), which constitutes the best method we found to ensure sample purity. Thus, a ^{15}N,^{13}C-C_2B domain sample that was subjected to our purification protocol but omitting the final cation exchange column still exhibited multiplicity for some of the cross-peaks from residues near the polybasic region (Figure 5B, black contours), despite not having the UV maximum at 260 nm characteristic of nucleic acids. This cross-peak

multiplicity shows that some contaminants remain bound to the polybasic region (49). Indeed, titatrions of this impure $^{15}N,^{13}C$-C_2B domain with SNARE complex monitored by 1D ^{13}C-edited ^{1}H-NMR spectra revealed a clearly weaker affinity (apparent K_d = 3.9 ± 1.0 μM) than analogous titrations with pure $^{15}N,^{13}C$-C_2B domain (apparent K_d = 0.80 ± 0.39 μM; Table 1) (see titration examples in Figure 5A).

Titrations of $^{15}N,^{13}C$-labeled C_2A domain with SNARE complex revealed a gradual decrease in SMR intensity that appeared to be saturable (Figure 5A), and fitting of the data suggested an apparent K_d of ca. 2 μM. However, because the decreases in SMR intensity were rather small, it is unclear whether saturation was indeed reached and hence whether this K_d value is reliable. The small decreases in SMR intensity suggest the existence of a loose binding mode whereby a small basic patch of the C_2A domain [perhaps in a Ca^{2+}-binding loop; see (42)] contacts an acidic region or regions of the SNARE complex, resulting in only limited immobilization of the C_2A domain. In contrast, the much stronger decrease in SMR intensity observed for the C_2B domain (Figure 5A) suggests the formation of a bona fide macromolecular assembly with the SNARE complex with a more extensive binding surface and considerable immobilization of the C_2B domain. This conclusion agrees with extensive evidence supporting the notion that synaptotagmin-1 binds to the SNARE complex primarily through the C_2B domain (38;39;41;46).

The KK mutation impairs the primary binding mode and the RR mutation impairs aggregation of SNARE complex/synaptotagmin-1 assemblies

To investigate which region(s) of the C_2B domain mediates binding to the SNARE complex, we performed titrations of $^{15}N,^{13}C$-labeled RR and KK C_2B domain mutants with the SNARE complex monitored by 1D ^{13}C-edited 1H-NMR spectra (Figure 6). Interestingly, the results were similar to those obtained in the titrations of the same mutants of the C_2AB fragment. Thus, in the titration performed with the C_2B domain RR mutant we obtained an apparent K_d (0.40 ± 0.30 μM; Table 1) that was lower than that derived for the WT C_2B domain, although we note that there is a considerable uncertainty in the mutant K_d because of intrinsic limitation of measuring K_d values below 1 μM by this method with the protein concentrations used. Nevertheless, the similarity with the results obtained for the C_2AB fragment is also manifested by the observation that the titration of the C_2B domain RR mutant saturated at substantially higher I_b value (0.51 ± 0.04; Table 1) than that observed for the WT C_2B domain (0.17 ± 0.05). Moreover, comparison of the 1D ^{13}C-edited ^{1}H-NMR spectra acquired in the presence of 20 μM SNARE complex again showed that the resonances from methyl groups in structured regions (e.g. between 0.4 and 0.6 ppm) remained observable for the C_2B domain RR mutant but not for the WT C_2B domain (Figure 7). Hence, these results suggest that the higher SNARE complex concentrations lead to formation of large complexes for the WT C_2B domain but such oligomerization is hindered by the RR mutation, thus leading to a 1:1 SNARE complex/C_2B domain assembly.

The results obtained with the C_2B domain KK mutant also resembled those obtained with the C_2AB fragment. Thus, the KK mutation in the C_2B domain again increased the apparent K_d measured (3.78 ± 1.99 μM) with respect to the WT C_2B domain K_d, without raising the I_b value. In fact, the calculated I_b for the C_2B domain KK mutant was close to 0 (−0.03 ± 0.09; Table 1), which can be attributed to the uncertainty in this value arising when saturation is not reached at the highest SNARE complex concentrations. Overall, these results show that the KK mutation in the polybasic region impairs the major SNARE complex binding mode while having much less effect, if any, on the oligomerization.

To test the conclusions emerging from the 1D NMR studies by another method, we performed precipitation assays with synaptotagmin-1 fragments and SNARE complex (Figure 8). For this purpose, we incubated 10 μM WT or mutant C_2AB fragment with 10 or

20 μM SNARE complex, separated the precipitate from the soluble fraction by centrifugation, and analyzed the samples by SDS PAGE. The results showed that, under both conditions, a substantial fraction of the C_2AB fragment precipitated and the RR mutation clearly decreased the precipitation (Figures 8A,C). The DN mutation appeared to somewhat decrease precipitation of the C_2AB fragment with the SNARE complex, but to a much lesser extent than the RR mutation. In contrast, the KK mutation did not impair precipitation. Similar results were obtained in precipitation assays with the WT or mutant C_2B domain and the SNARE complex, and in this case the inhibition of the precipitation by the RR mutation was even more dramatic (Figures 8B,D; note that the C_2B domain runs below the SNARE complex in the gels, in contrast to the C_2AB fragment). It is worth noting that the isolated C_2AB fragment, the isolated C_2B domain and the isolated SNARE complex are highly soluble and yield excellent NMR data at concentrations much higher than those used in these experiments (12;22;49;50;52). Hence, the precipitation results arise from the tendency of the synaptotagmin-1 fragments to aggregate with the SNARE complex.

DISCUSSION

Synaptotagmin-1/SNARE interactions are widely believed to be critical for coupling Ca^{2+} sensing to membrane fusion during neurotransmitter release. Despite dozens of papers describing such interactions, it has been difficult to characterize them with quantitative biophysical methods and to define the binding sites involved. Because synaptotagmin-1 acts at the final, Ca^{2+}-triggering step of release, its interactions with the SNARE complex are likely to be particularly important. Here we have used 1D ^{13}C-edited 1H-NMR spectra to shed light into the nature of SNARE complex/synaptotagmin-1 interactions. Our results underline the difficulties involved in the analysis of such interactions, showing that the tendency of synaptotagmin-1 fragments to aggregate with the SNARE complex can severely hinder interpretation of the results. Moreover, our data reveal that the two arginines at the bottom of the C_2B domain contribute to this aggregation tendency and strongly support the notion that the polybasic region of the C_2B domain constitutes the primary binding site for the SNARE complex.

The propensity of SNARE complex/synaptotagmin-1 assemblies to aggregate in the presence of Ca^{2+} has hindered application of the standard two-dimensional (2D) heteronuclear NMR methods that can be used to readily map the binding sites involved in protein complexes (47). Even in the absence of Ca^{2+}, analysis of SNARE complex/C_2AB fragment interactions by TROSY-HSQC spectra revealed multiple binding sites (41) that probably reflect the formation of oligomeric assemblies at the protein concentrations used for these experiments (≥ 40 μM). Application of 1D NMR techniques has a clear disadvantage from the point of view of resolution, as it leads to loss of most of the residue specific information on binding. However, 1D NMR spectra exhibit a dramatic gain in sensitivity at regions where multiple resonances overlap, particular at the most intense methyl region that we refer to as SMR. Such gain in sensitivity, combined with the use of ^{13}C-editing to select the ^{1}H signals of only the ^{13}C-labeled protein, allowed us to analyze SNARE complex interactions at concentrations of synaptotagmin-1 fragments in the 3 μM range.

While such concentrations of synaptotagmin-1 fragments prevent precipitation, our titrations monitored by 1D ^{13}C-edited ^{1}H-NMR spectra show that the higher SNARE complex concentrations still lead to the formation of large oligomeric complexes with the WT C_2AB fragment or C_2B domain, which can naturally be assumed to reflect the same phenomena that lead to precipitation at concentrations of synaptotagmin-1 fragments of 10 μM or higher. Our titrations also show that the RR and KK mutations in the bottom and the polybasic region of the C_2B domain, respectively, have different effects on the underlying

interactions. The RR mutation hinders formation of large complexes and strongly hinders precipitation, leading to titration curves that most likely correspond to SNARE complex/synaptotagmin-1 fragment binding with 1:1 stoichiometry. Hence, while the titrations performed with the WT synaptotagmin-1 fragments cannot be used to derive dissociation constants readily, those performed with the C_2AB and C_2B RR mutants provide more reliable data to estimate the affinity involved in the primary binding mode with the SNARE complex. It is still difficult to calculate accurate K_ds from these titrations when the interaction under study is relatively tight because of the need to use concentrations of the unlabeled protein in the μM range, but the K_d values calculated from these titrations (0.94 ± 0.01 and 0.40 ± 0.30; Table 1) suggest that the actual dissociation constant is 1 μM or lower.

As concluded for the WT titrations, the K_ds measured with the C_2AB and C_2B KK mutants cannot be considered reliable because the KK mutation does not have a clear effect in preventing aggregation, if any. However, it is clear that the KK mutation impairs the primary binding mode between synaptotagmin-1 and the SNARE complex based on the smaller decreases in SMR intensities observed at low SNARE complex concentrations for both the C_2AB fragment (Figure 3D) and for the C_2B domain (Figure 6B), compared to the titrations using WT fragments. These results and those obtained with the RR mutation strongly support the notion that the primary binding mode involves the polybasic region of the C_2B domain but not the bottom region of the C_2B domain. This conclusion agrees with some of the previous studies (23;41;44) but not others (45;46). Thus, while the existence of such a primary binding site as concluded from our data might seem trivial, it was not obvious from the available literature and is very important to understand how the functions of synaptotagmin-1 and SNAREs are coupled. Note also that much of the surface of the SNARE complex is highly negative (7;55) whereas most of the synaptotagmin-1 C_2B domain and part of the C_2A domain are highly positive upon Ca^{2+} binding (10;12;41). This observation, together with the high tendency of C_2AB fragment/SNARE complexes to aggregate, and reports implicating different regions of both the SNARE complex and synaptotagmin-1 in binding (see Introduction), raised the possibility that the reported interactions might not be specific, or that there might be multiple binding modes with comparable affinities. Such features would strongly hinder the development of well-defined models for synaptotagmin-1/SNARE coupling as well as testing of these models. Our data now show that it is possible to disentangle the primary binding mode between synaptotagmin-1 and the SNARE complex from other interactions that favor oligomerization.

The contributions of the C_2A domain to SNARE complex binding are still somewhat unclear. The titrations of the isolated C_2A domain with SNARE complex (Figure 5A) indicate that the C_2A domain does not have an extensive, intimate interaction with the SNARE complex, in contrast to the C_2B domain. However, there appears to be some dynamic interaction that may involve a small surface of the C_2A domain. This interaction may be disrupted by the DN mutation in the Ca^{2+}-binding loops of the C_2A domain. The DN mutation had a similar effect on the titrations of the C_2AB fragment with the SNARE complex as that caused by the RR mutation (Figure 3), but the DN mutation did not impair precipitation with the SNARE complex, at least to the extent observed for the RR mutation (Figure 8). Nevertheless, it is still plausible that interactions of the C_2A domain Ca^{2+}-binding loops with the SNARE complex add to those involving the polybasic region and/or the bottom of the C_2B domain to provide multivalency and hence favor formation of SNARE complex/C_2AB fragment oligomers.

It is important to emphasize that the results presented here were obtained in the absence of membranes and that binding of synaptotagmin-1 to membranes most likely influences its interactions with the SNARE complex (40;41). Interestingly however, the conclusions

derived from our data correlate well with results obtained in studies of how the synaptotagmin-1 C_2AB fragment competes with complexin-I for binding to membrane-anchored SNARE complex, which showed that the KK mutation in the polybasic region of the C_2B domain impairs complexin-I displacement by the C_2AB fragment (41). In contrast, the RR mutation did not alter this activity but impaired the ability of the C_2AB fragment or the C_2B domain to bridge two membranes (22;23). All these results are consistent with a model whereby the polybasic region on the side of the synaptotagmin-1 C_2B domain binds to the SNARE complex and this interaction places synaptotagmin-1 in an orientation that naturally allows binding of the Ca^{2+}-binding loops at the top of both C_2 domains to one membrane and the arginines at the bottom of the C_2B domain to another, closely apposed membrane (41).

This model provides a clear explanation for the dramatic impairment of neurotransmitter release caused by the RR mutation and for the function of synaptotagmin-1 in cooperating with the SNAREs in inducing fast membrane fusion (22;23). Hence, it seems likely that membranes are the true physiological targets of the two arginines at the bottom of the C_2B domain and of the C_2A domain Ca^{2+}-binding region, and that, in the absence of membranes, these positively charged regions are avid for binding to negatively charged surfaces such as those present around much of the SNARE complex. Such avidity could explain the participation of the two arginines and at the bottom of the C_2B domain and of the C_2A domain Ca^{2+}-binding region in the aggregation of the C_2AB fragment with the SNARE complex in solution. Note also that the observation of oligomerization and/or precipitation of protein complexes very often lacks physiological significance and just reflects insolubility. Nevertheless, we cannot rule out the possibility that SNARE complex/synaptotagmin-1 oligomers are functionally important and that disruption of such oligomers underlies the functional effects of the RR mutation. In fact, this alternative possibility is supported by the correlation between the strong effects of the RR mutation on C_2AB fragment/SNARE complex aggregation and on neurotransmitter release. Clearly, multiple questions remain about how SNARE complex/synaptotagmin-1 interactions control neurotransmitter release. The results presented here show that disentangling the primary binding mode from additional interactions is crucial to address these questions, and that 1D NMR methods provide a powerful tool for this purpose.

Acknowledgments

We thank Yilun Sun for expert technical assistance and Alpay B. Seven for fruitful discussions.

Abbreviations

1D	one dimensional
2D	two dimensional
HSQC	heteronuclear single quantum correlation
NMR	nuclear magnetic resonance
RT	room temperature
SMR	strongest methyl resonance
SNARE	soluble N-ethylmaleimide sensitive factor attachment protein receptor
TROSY	transverse relaxation optimized spectroscopy
WT	wild type

REFERENCES

1. Brunger AT. Structure and function of SNARE and SNARE-interacting proteins. Q.Rev. Biophys. 2005:1–47. [PubMed: 16336742]
2. Sorensen JB. Conflicting views on the membrane fusion machinery and the fusion pore. Annu.Rev. Cell Dev. Biol. 2009; 25:513–537. [PubMed: 19575641]
3. Jahn R, Fasshauer D. Molecular machines governing exocytosis of synaptic vesicles. Nature. 2012; 490:201–207. [PubMed: 23060190]
4. Rizo J, Sudhof TC. The Membrane Fusion Enigma: SNAREs, Sec1/Munc18 Proteins, and Their Accomplices-Guilty as Charged? Annu.Rev. Cell Dev. Biol. 2012; 28:279–308. [PubMed: 23057743]
5. Ma C, Su L, Seven AB, Xu Y, Rizo J. Reconstitution of the vital functions of Munc18 and Munc13 in neurotransmitter release. Science. 2013; 339:421–425. [PubMed: 23258414]
6. Poirier MA, Xiao W, Macosko JC, Chan C, Shin YK, Bennett MK. The synaptic SNARE complex is a parallel four-stranded helical bundle. Nat.Struct. Biol. 1998; 5:765–769. [PubMed: 9731768]
7. Sutton RB, Fasshauer D, Jahn R, Brunger AT. Crystal structure of a SNARE complex involved in synaptic exocytosis at 2.4 A resolution. Nature. 1998; 395:347–353. [PubMed: 9759724]
8. Hanson PI, Roth R, Morisaki H, Jahn R, Heuser JE. Structure and conformational changes in NSF and its membrane receptor complexes visualized by quick-freeze/deep-etch electron microscopy. Cell. 1997; 90:523–535. [PubMed: 9267032]
9. Sutton RB, Davletov BA, Berghuis AM, Sudhof TC, Sprang SR. Structure of the first C2 domain of synaptotagmin I: a novel Ca2+/phospholipid-binding fold. Cell. 1995; 80:929–938. [PubMed: 7697723]
10. Ubach J, Zhang X, Shao X, Sudhof TC, Rizo J. Ca2+ binding to synaptotagmin: how many Ca2+ ions bind to the tip of a C2-domain? EMBO J. 1998:17, 3921–3930.
11. Shao X, Fernandez I, Sudhof TC, Rizo J. Solution structures of the Ca2+-free and Ca2+-bound C2A domain of synaptotagmin I: does Ca2+ induce a conformational change? Biochemistry. 1998; 37:16106–16115. [PubMed: 9819203]
12. Fernandez I, Arac D, Ubach J, Gerber SH, Shin O, Gao Y, Anderson RG, Sudhof TC, Rizo J. Three-dimensional structure of the synaptotagmin 1 c(2)b-domain. Synaptotagmin 1 as a phospholipid binding machine. Neuron. 2001; 32:1057–1069. [PubMed: 11754837]
13. Chapman ER, Davis AF. Direct interaction of a Ca2+-binding loop of synaptotagmin with lipid bilayers. J.Biol. Chem. 1998; 273:13995–14001. [PubMed: 9593749]
14. Zhang X, Rizo J, Sudhof TC. Mechanism of phospholipid binding by the C2A-domain of synaptotagmin I. Biochemistry. 1998; 37:12395–12403. [PubMed: 9730811]
15. Fernandez-Chacon R, Konigstorfer A, Gerber SH, Garcia J, Matos MF, Stevens CF, Brose N, Rizo J, Rosenmund C, Sudhof TC. Synaptotagmin I functions as a calcium regulator of release probability. Nature. 2001; 410:41–49. [PubMed: 11242035]
16. Rhee JS, Li LY, Shin OH, Rah JC, Rizo J, Sudhof TC, Rosenmund C. Augmenting neurotransmitter release by enhancing the apparent Ca2+ affinity of synaptotagmin 1. Proc. Natl. Acad. Sci. U. S. A. 2005; 102:18664–18669. [PubMed: 16352718]
17. Mackler JM, Drummond JA, Loewen CA, Robinson IM, Reist NE. The C(2)B Ca(2+)-binding motif of synaptotagmin is required for synaptic transmission in vivo. Nature. 2002; 418:340–344. [PubMed: 12110842]
18. Nishiki T, Augustine GJ. Dual roles of the C2B domain of synaptotagmin I in synchronizing Ca2+-dependent neurotransmitter release. J. Neurosci. 2004; 24:8542–8550. [PubMed: 15456828]
19. Robinson IM, Ranjan R, Schwarz TL. Synaptotagmins I and IV promote transmitter release independently of Ca(2+) binding in the C(2)A domain. Nature. 2002; 418:336–340. [PubMed: 12110845]
20. Fernandez-Chacon R, Shin OH, Konigstorfer A, Matos MF, Meyer AC, Garcia J, Gerber SH, Rizo J, Sudhof TC, Rosenmund C. Structure/function analysis of Ca2+ binding to the C2A domain of synaptotagmin 1. J. Neurosci. 2002; 22:8438–8446. [PubMed: 12351718]

21. Shin OH, Xu J, Rizo J, Sudhof TC. Differential but convergent functions of Ca2+ binding to synaptotagmin-1 C2 domains mediate neurotransmitter release. Proc. Natl. Acad. Sci. U. S. A. 2009; 106:16469–16474. [PubMed: 19805322]
22. Arac D, Chen X, Khant HA, Ubach J, Ludtke SJ, Kikkawa M, Johnson AE, Chiu W, Sudhof TC, Rizo J. Close membrane-membrane proximity induced by Ca(2+)-dependent multivalent binding of synaptotagmin-1 to phospholipids. Nat. Struct. Mol. Biol. 2006; 13:209–217. [PubMed: 16491093]
23. Xue M, Ma C, Craig TK, Rosenmund C, Rizo J. The Janus-faced nature of the C(2)B domain is fundamental for synaptotagmin-1 function. Nat. Struct. Mol. Biol. 2008; 15:1160–1168. [PubMed: 18953334]
24. Bai J, Tucker WC, Chapman ER. PIP2 increases the speed of response of synaptotagmin and steers its membrane-penetration activity toward the plasma membrane. Nat. Struct. Mol. Biol. 2004; 11:36–44. [PubMed: 14718921]
25. Mackler JM, Reist NE. Mutations in the second C2 domain of synaptotagmin disrupt synaptic transmission at Drosophila neuromuscular junctions. J. Comp Neurol. 2001; 436:4–16. [PubMed: 11413542]
26. Li L, Shin OH, Rhee JS, Arac D, Rah JC, Rizo J, Sudhof T, Rosenmund C. Phosphatidylinositol phosphates as co-activators of Ca2+ binding to C2 domains of synaptotagmin 1. J. Biol. Chem. 2006; 281:15845–15852. [PubMed: 16595652]
27. Bennett MK, Calakos N, Scheller RH. Syntaxin: a synaptic protein implicated in docking of synaptic vesicles at presynaptic active zones. Science. 1992; 257:255–259. [PubMed: 1321498]
28. Li C, Ullrich B, Zhang JZ, Anderson RG, Brose N, Sudhof TC. Ca(2+)-dependent and -independent activities of neural and non-neural synaptotagmins. Nature. 1995; 375:594–599. [PubMed: 7791877]
29. Chapman ER, Hanson PI, An S, Jahn R. Ca2+ regulates the interaction between synaptotagmin and syntaxin 1. J. Biol. Chem. 1995; 270:23667–23671. [PubMed: 7559535]
30. Kee Y, Scheller RH. Localization of synaptotagmin-binding domains on syntaxin. J. Neurosci. 1996; 16:1975–1981. [PubMed: 8604041]
31. Shao X, Li C, Fernandez I, Zhang X, Sudhof TC, Rizo J. Synaptotagmin-syntaxin interaction: the C2 domain as a Ca2+-dependent electrostatic switch. Neuron. 1997; 18:133–142. [PubMed: 9010211]
32. Fernandez I, Ubach J, Dulubova I, Zhang X, Sudhof TC, Rizo J. Three-dimensional structure of an evolutionarily conserved N-terminal domain of syntaxin 1A. Cell. 1998; 94:841–849. [PubMed: 9753330]
33. Matos MF, Rizo J, Sudhof TC. The relation of protein binding to function: what is the significance of munc18 and synaptotagmin binding to syntaxin 1, and where are the corresponding binding sites? Eur. J. Cell Biol. 2000; 79:377–382. [PubMed: 10928452]
34. Davis AF, Bai J, Fasshauer D, Wolowick MJ, Lewis JL, Chapman ER. Kinetics of synaptotagmin responses to Ca2+ and assembly with the core SNARE complex onto membranes. Neuron. 1999; 24:363–376. [PubMed: 10571230]
35. Gerona RR, Larsen EC, Kowalchyk JA, Martin TF. The C terminus of SNAP25 is essential for Ca(2+)-dependent binding of synaptotagmin to SNARE complexes. J. Biol. Chem. 2000; 275:6328–6336. [PubMed: 10692432]
36. Zhang X, Kim-Miller MJ, Fukuda M, Kowalchyk JA, Martin TF. Ca2+-dependent synaptotagmin binding to SNAP-25 is essential for Ca2+-triggered exocytosis. Neuron. 2002; 34:599–611. [PubMed: 12062043]
37. Rickman C, Davletov B. Mechanism of calcium-independent synaptotagmin binding to target SNAREs. J. Biol. Chem. 2003; 278:5501–5504. [PubMed: 12496268]
38. Rickman C, Archer DA, Meunier FA, Craxton M, Fukuda M, Burgoyne RD, Davletov B. Synaptotagmin interaction with the syntaxin/SNAP-25 dimer is mediated by an evolutionarily conserved motif and is sensitive to inositol hexakisphosphate. J. Biol. Chem. 2004; 279:12574–12579. [PubMed: 14709554]

39. Bowen ME, Weninger K, Ernst J, Chu S, Brunger AT. Single- molecule studies of synaptotagmin and complexin binding to the SNARE complex. Biophys. J. 2005; 89:690–702. [PubMed: 15821166]
40. Tang J, Maximov A, Shin OH, Dai H, Rizo J, Sudhof TC. A complexin/synaptotagmin 1 switch controls fast synaptic vesicle exocytosis. Cell. 2006; 126:1175–1187. [PubMed: 16990140]
41. Dai H, Shen N, Arac D, Rizo J. A Quaternary SNARE-Synaptotagmin- Ca(2+)-Phospholipid Complex in Neurotransmitter Release. J. Mol. Biol. 2007; 367:848–863. [PubMed: 17320903]
42. Lynch KL, Gerona RR, Larsen EC, Marcia RF, Mitchell JC, Martin TF. Synaptotagmin C2A loop 2 mediates Ca2+-dependent SNARE interactions essential for Ca2+-triggered vesicle exocytosis. Mol. Biol. Cell. 2007; 18:4957–4968. [PubMed: 17914059]
43. Rizo J, Chen X, Arac D. Unraveling the mechanisms of synaptotagmin and SNARE function in neurotransmitter release. Trends Cell Biol. 2006; 16:339–350. [PubMed: 16698267]
44. Rickman C, Jimenez JL, Graham ME, Archer DA, Soloviev M, Burgoyne RD, Davletov B. Conserved prefusion protein assembly in regulated exocytosis. Mol. Biol. Cell. 2006; 17:283–294. [PubMed: 16267273]
45. Gaffaney JD, Dunning FM, Wang Z, Hui E, Chapman ER. Synaptotagmin C2B domain regulates Ca2+-triggered fusion in vitro: critical residues revealed by scanning alanine mutagenesis. J. Biol. Chem. 2008; 283:31763–31775. [PubMed: 18784080]
46. Choi UB, Strop P, Vrljic M, Chu S, Brunger AT, Weninger KR. Single-molecule FRET-derived model of the synaptotagmin 1-SNARE fusion complex. Nat. Struct. Mol. Biol. 2010; 17:318–324. [PubMed: 20173763]
47. Rizo J, Rosen MK, Gardner KH. Enlightening molecular mechanisms through study of protein interactions. J. Mol. Cell Biol. 2012; 4:270–283. [PubMed: 22735643]
48. Arac D, Murphy T, Rizo J. Facile detection of protein-protein interactions by one-dimensional NMR spectroscopy. Biochemistry. 2003; 42:2774–2780. [PubMed: 12627942]
49. Ubach J, Lao Y, Fernandez I, Arac D, Sudhof TC, Rizo J. The C2B domain of synaptotagmin I is a Ca2+-binding module. Biochemistry. 2001; 40:5854–5860. [PubMed: 11352720]
50. Chen X, Tomchick DR, Kovrigin E, Arac D, Machius M, Sudhof TC, Rizo J. Three-dimensional structure of the complexin/SNARE complex. Neuron. 2002; 33:397–409. [PubMed: 11832227]
51. Shao X, Davletov BA, Sutton RB, Sudhof TC, Rizo J. Bipartite Ca2+-binding motif in C2 domains of synaptotagmin and protein kinase C. Science. 1996; 273:248–251. [PubMed: 8662510]
52. Chen X, Tang J, Sudhof TC, Rizo J. Are neuronal SNARE proteins Ca2+ sensors? J. Mol. Biol. 2005; 347:145–158. [PubMed: 15733924]
53. Pang ZP, Shin OH, Meyer AC, Rosenmund C, Sudhof TC. A gainof-function mutation in synaptotagmin-1 reveals a critical role of Ca2+-dependent soluble N-ethylmaleimide-sensitive factor attachment protein receptor complex binding in synaptic exocytosis. J. Neurosci. 2006; 26:12556–12565. [PubMed: 17135417]
54. Shao X, Sudhof TC, Rizo J. Assignment of the 1H, 15N and 13C resonances of the calcium-free and calcium-bound forms of the first C2-domain of synaptotagmin I. J. Biomol. NMR. 1997; 10:307–308. [PubMed: 9390409]
55. Fasshauer D, Sutton RB, Brunger AT, Jahn R. Conserved structural features of the synaptic fusion complex: SNARE proteins reclassified as Q- and RSNAREs. Proc. Natl. Acad. Sci. U. S. A. 1998; 95:15781–15786. [PubMed: 9861047]

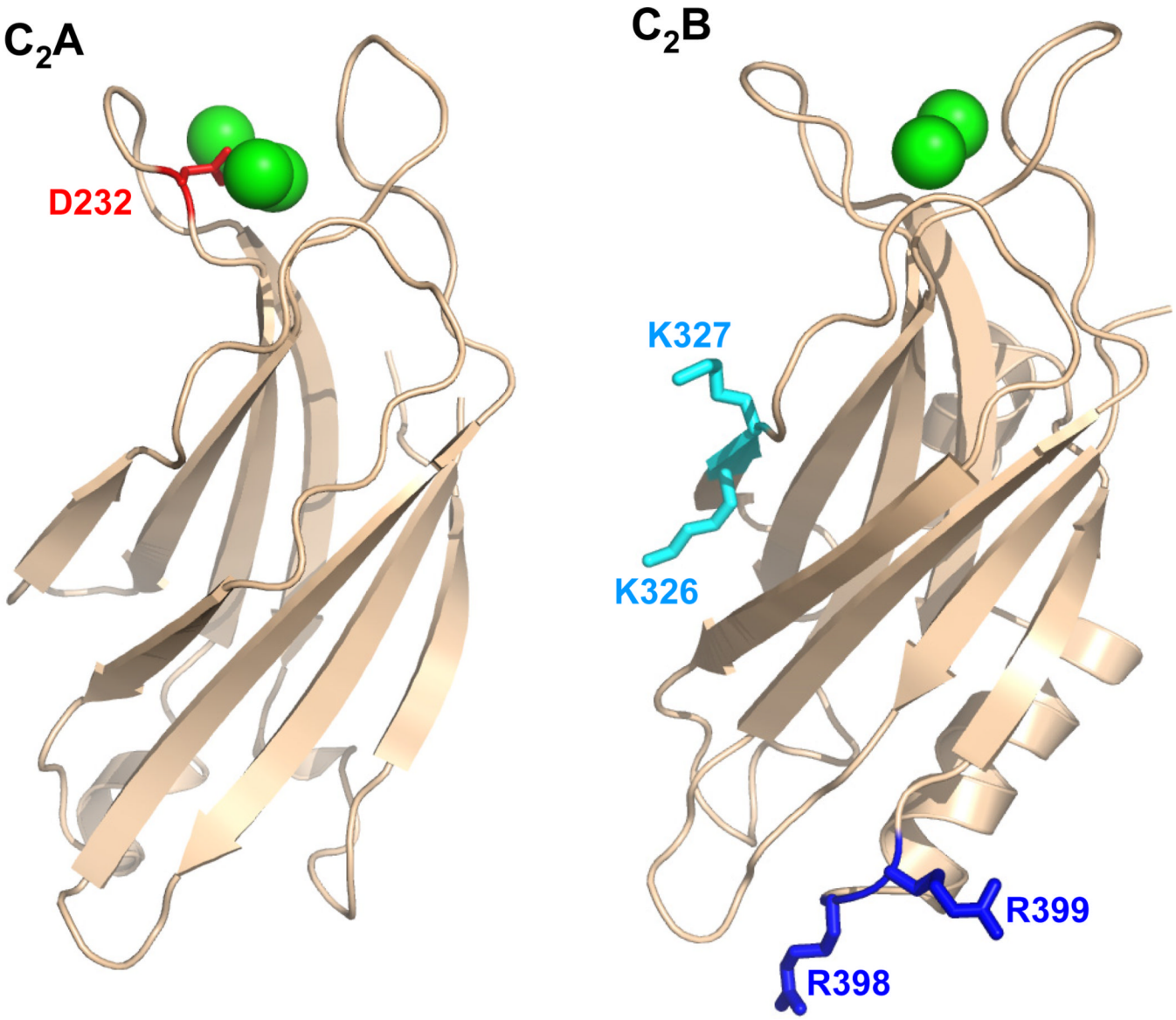

Figure 1.
Ribbon diagrams of the synaptotagmin-1 C_2A and C_2B domains. Ca^{2+} ions are shown as green spheres. The side chains that were mutated are represented by stick models and labeled.

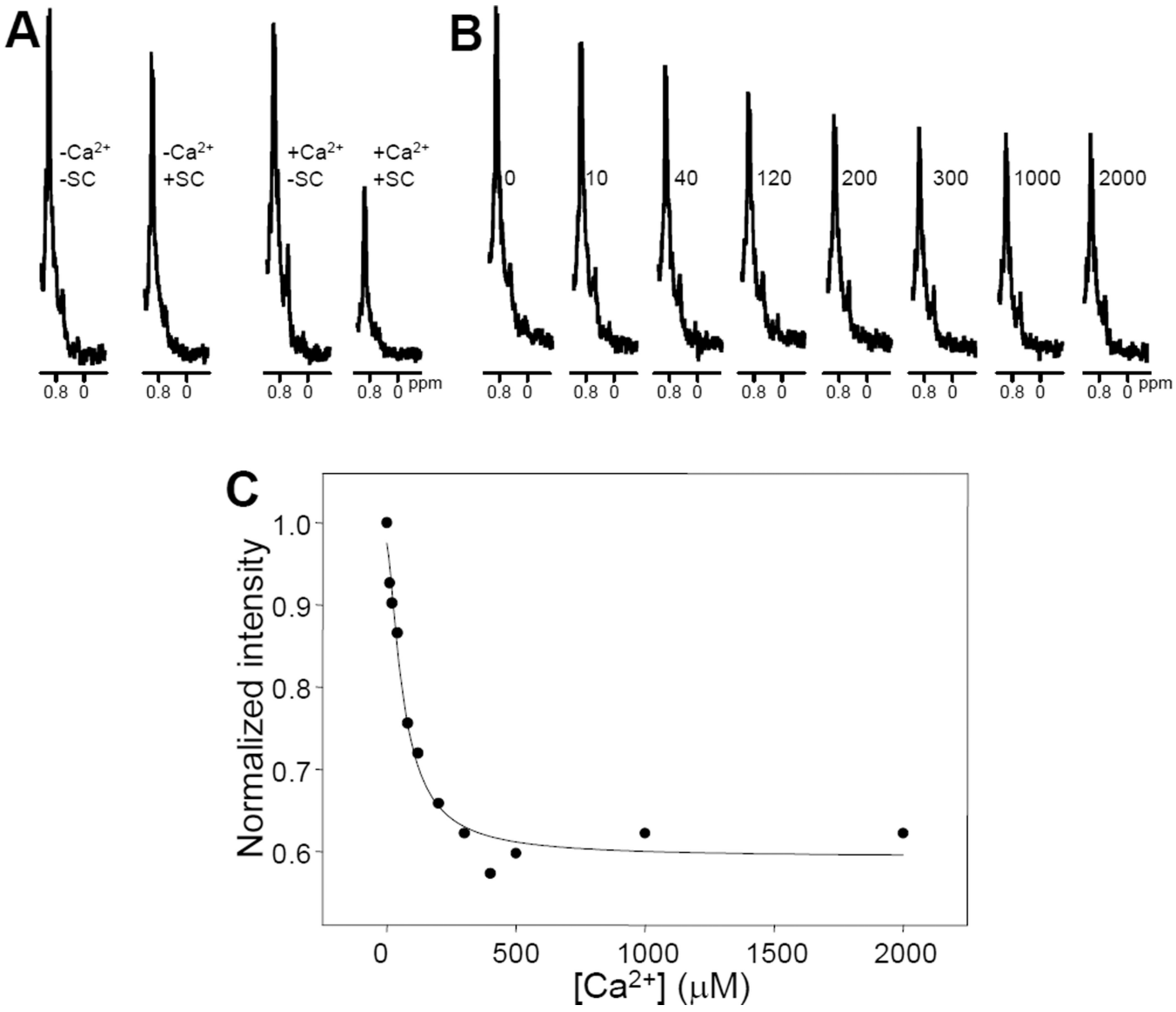

Figure 2.

A. Expansions of the region containing the SMR of 1D ^{13}C-edited ^{1}H-NMR spectra of 3 μM $^{15}N,^{13}C$-labeled C_2AB fragment acquired in the presence of 1 mM EDTA (-Ca^{2+}) or 1 mM Ca^{2+} (+Ca^{2+}), and in the absence (−SC) or presence (+SC) of 3.5 μM SNARE complex. **B**. analogous expansions of 1D ^{13}C-edited 1H-NMR spectra of 3 μM $^{15}N,^{13}C$-labeled C_2AB fragment in the presence of 3.5 μM SNARE complex and the indicated concentrations of Ca^{2+} in μM units. **C**. Plot of the normalized SMR intensities observed in 1D ^{13}C-edited ^{1}H-NMR spectra of 3 μM $^{15}N,^{13}C$-labeled C_2AB fragment in the presence of 3.5 μM SNARE complex and variable concentrations of Ca^{2+}. A subset of the data corresponding to this titration is shown in panel **B**. The curve shows the fit to a Hill equation.

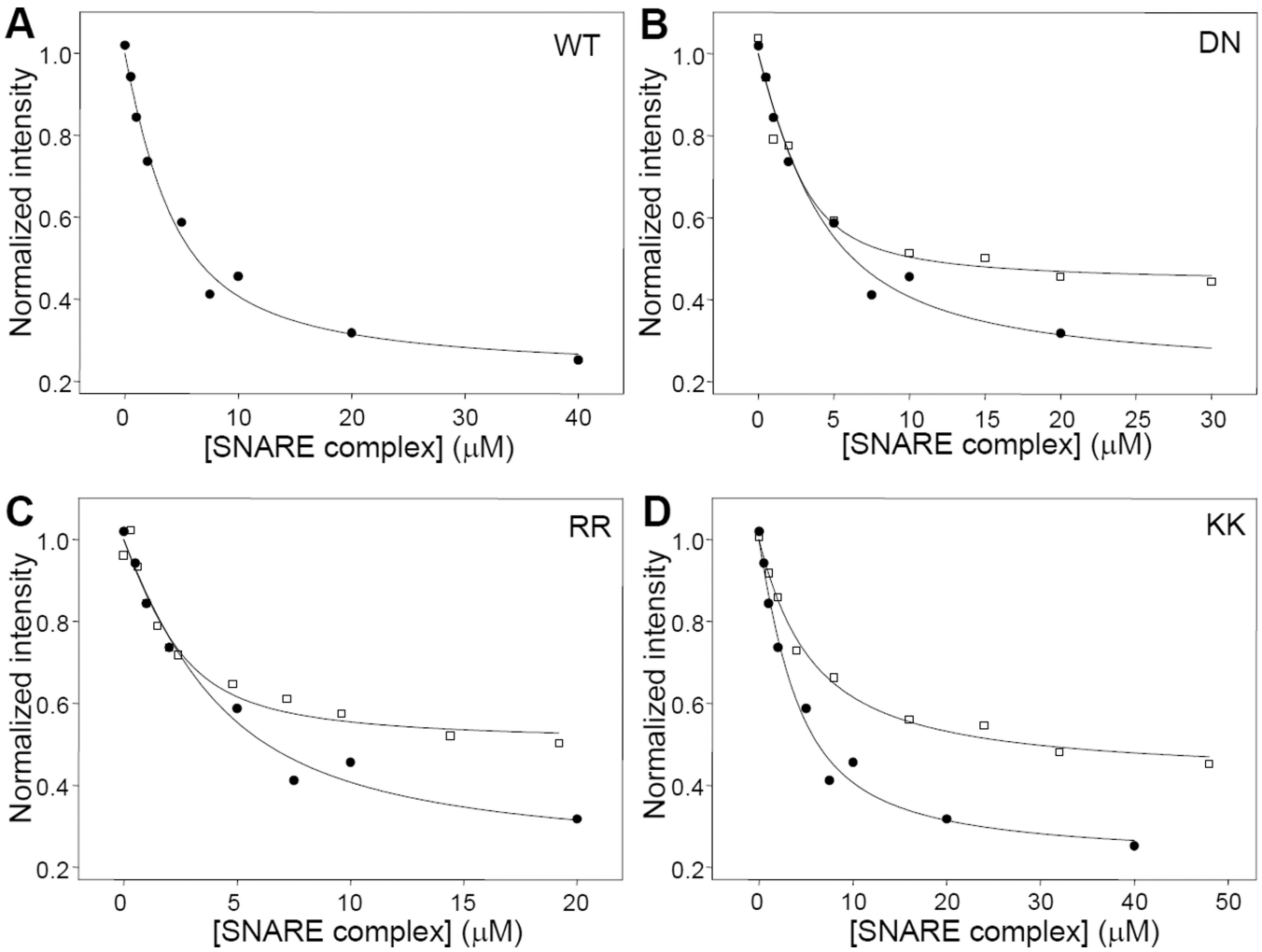

Figure 3.

Titrations of WT and mutant $^{15}N,^{13}C$-labeled C_2AB fragments with SNARE complex monitored by 1D ^{13}C-edited ^{1}H-NMR spectra. **A**. Plot of the SMR intensities observed in 1D ^{13}C-edited ^{1}H-NMR spectra of 3 μM WT C_2AB fragment as a function of unlabeled SNARE complex concentration in the presence of 1 mM Ca^{2+}. **B-D**. Plots for analogous titrations performed with DN (**B**), RR (**C**) and KK (**D**) mutant C_2AB fragments (open squares), superimposed with a plot obtained for the WT C_2AB fragment (closed circles; the same shown in **A**). The curves show the fits of the data obtained with equation (1).

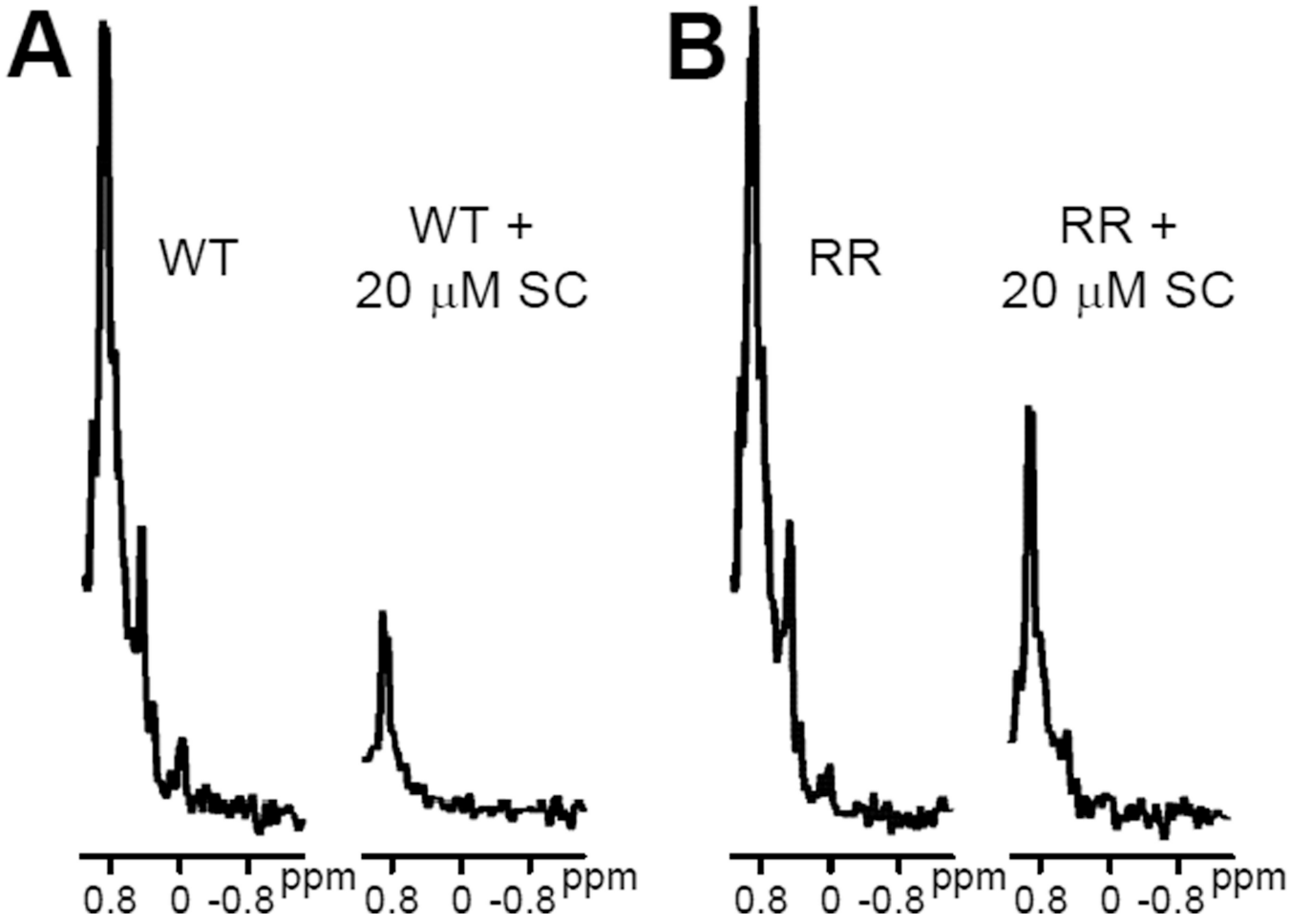

Figure 4.

Expansions showing the methyl region of 1D ^{13}C-edited 1H-NMR spectra of 3 μM WT (**A**) or RR mutant (**B**) C_2AB fragment in 1 mM Ca^{2+} and in the absence or presence of 20 μM SNARE complex (SC).

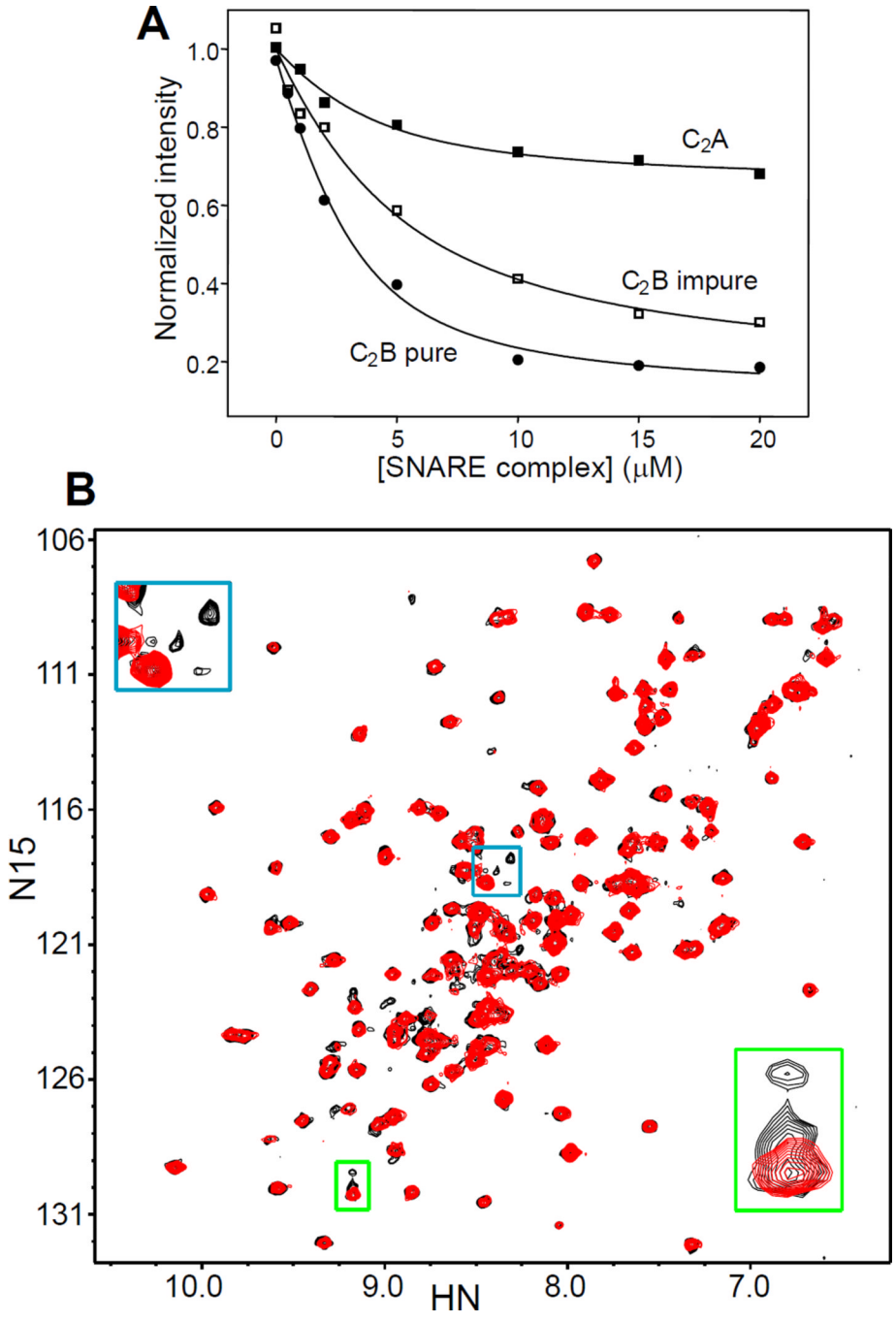

Figure 5.

Analysis of the relative contributions of the synaptotagmin-1 C_2 domains to SNARE complex binding. **A**. Plots of the SMR intensities observed in 1D ^{13}C-edited ^{1}H-NMR spectra of 3 μM synaptotagmin-1 C_2A domain (solid squares), pure C_2B domain (solid cirlces) and impure C_2B domain (open squares) as a function of unlabeled SNARE complex concentration in the presence of 1 mM Ca^{2+}. **B**. ^{1}H-^{15}N HSQC spectra of synaptotagmin-1 C_2B domain that was fully purified (red contours) or that was purified by our standard protocol but omitting the final cation exchange chromatography (black contours). The insets

show expansions of regions containing cross-peaks that are unique for the purified C_2B domain but exhibit multiplicity in the impure C_2B domain [see ref. (49)].

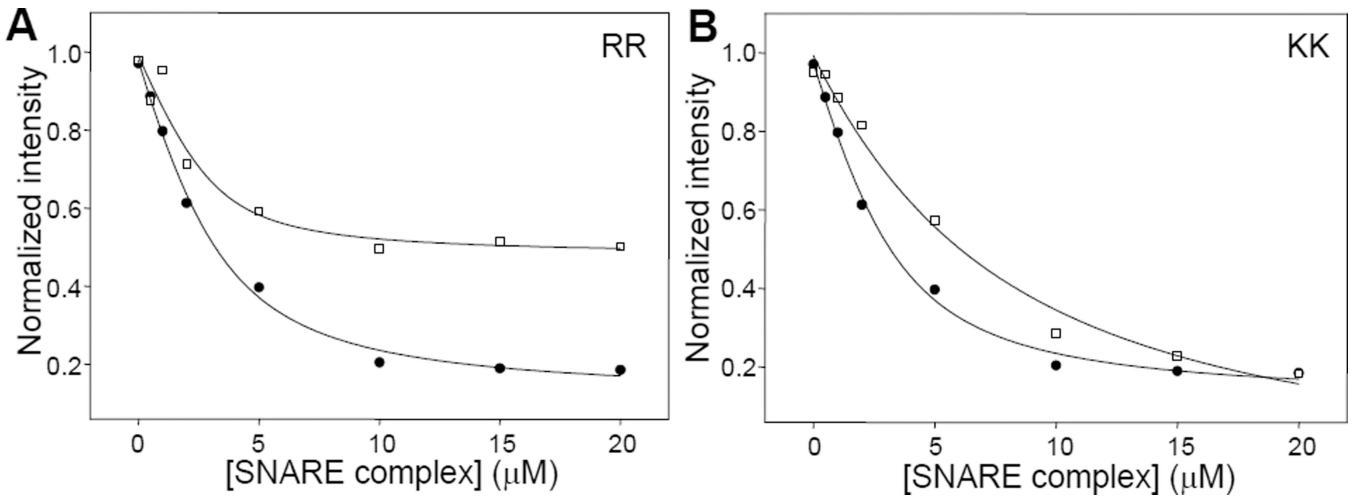

Figure 6.

Titrations of WT and mutant $^{15}N,^{13}C$-labeled C_2B domain with SNARE complex monitored by 1D ^{13}C-edited 1H-NMR spectra. **A–B**. Plots of the SMR intensities observed in 1D ^{13}C-edited ^{1}H-NMR spectra of 3 μM $^{15}N,^{13}C$-labeled RR (**A**) or KK (**B**) mutant C_2B domain as a function of unlabeled SNARE complex concentration in the presence of 1 mM Ca^{2+} (open squares), superimposed with a plot obtained for the WT C_2B domain (closed circles). The curves show the fits of the data obtained with equation (1).

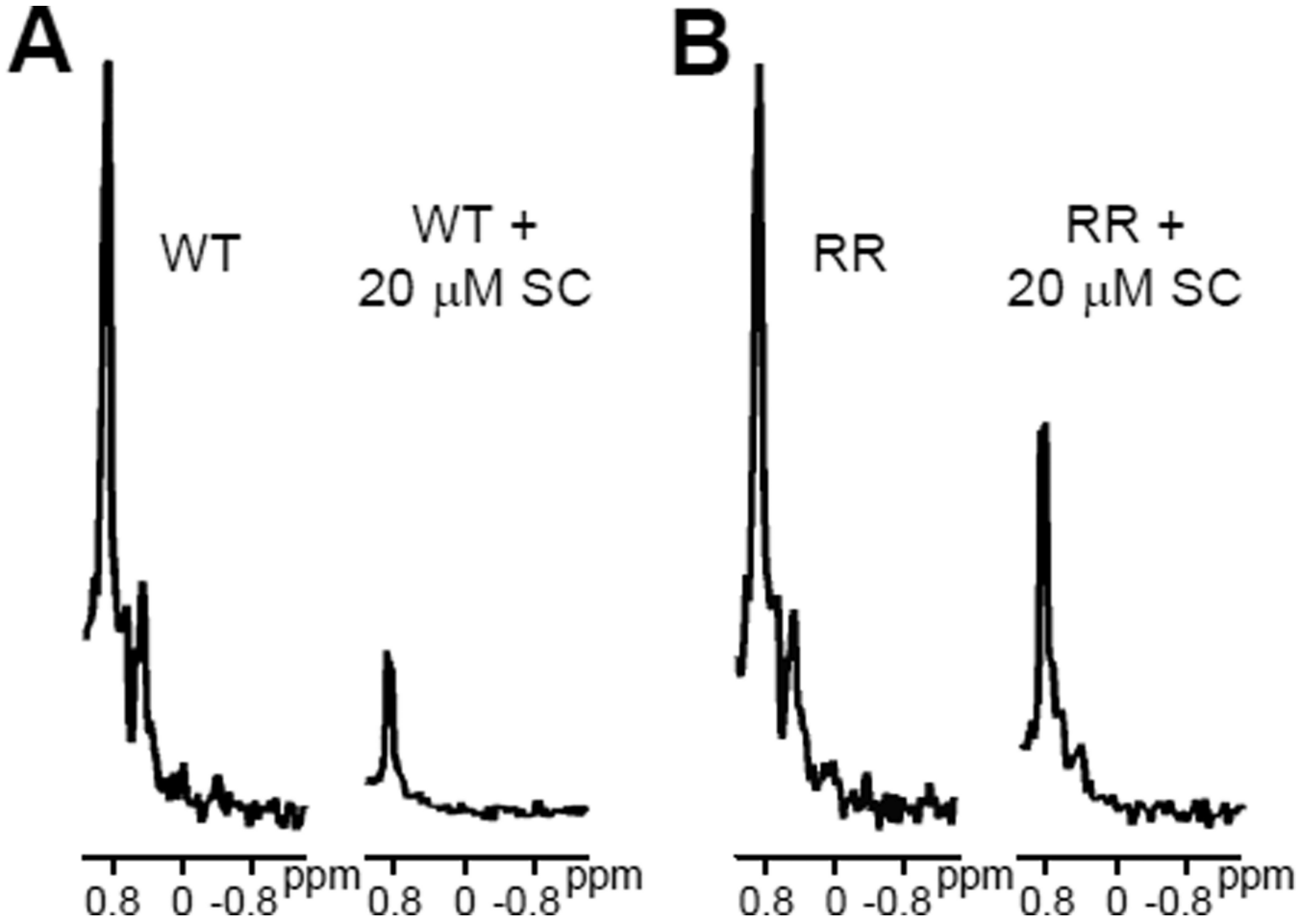

Figure 7.

Expansions showing the methyl region of 1D ^{13}C-edited ^{1}H-NMR spectra of 3 μM WT (**A**) or RR mutant (**B**) C2B domain in 1 mM Ca^{2+} and in the absence or presence of 20 μM SNARE complex (SC).

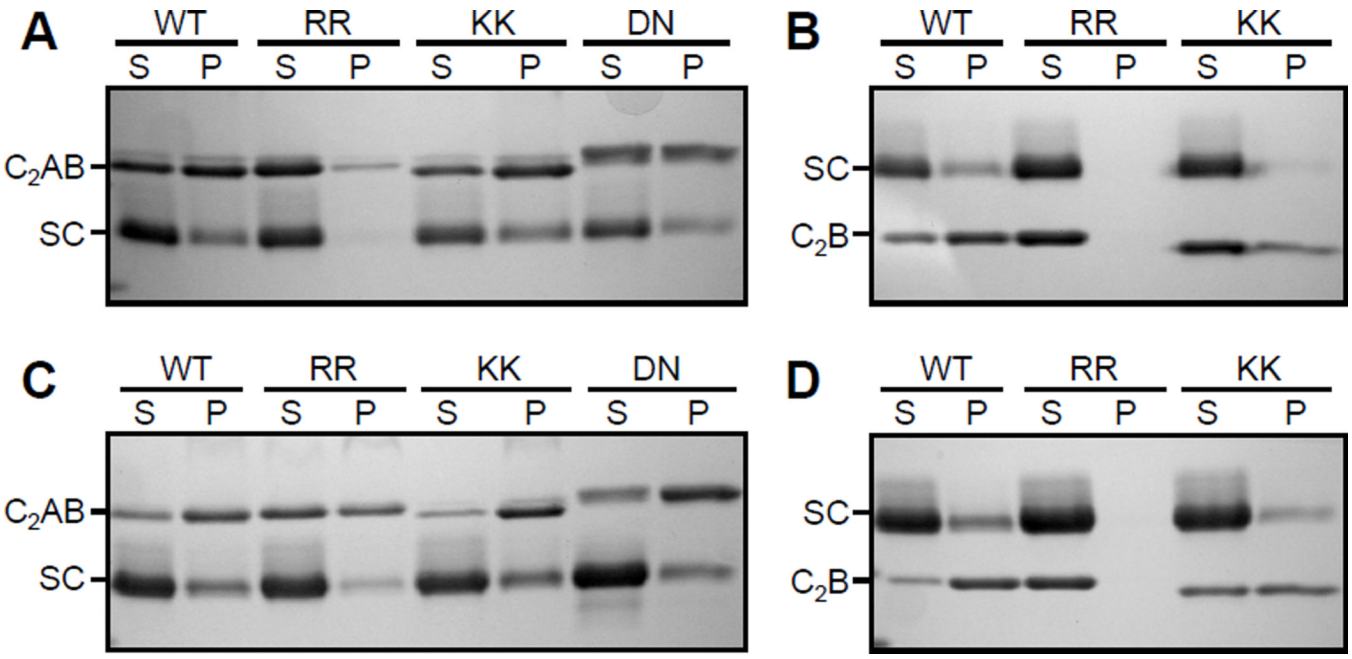

Figure 8.

Analysis of the solubility of WT and mutant synaptotagmin-1 fragments in the presence of SNARE complex. Samples containing 10 μM C_2AB fragment (**A,C**) or 10 μM C_2B domain (**B,D**) were incubated with 10 μM (**A,B**) or 20 μM (**C,D**) SNARE complex for 5 min in the presence of 1 mM Ca^{2+}. The soluble fractions (S) and the precipitates (P) were separated by centrifugation and analyzed by SDS PAGE followed by Coomassie blue staining. The positions of the C_2AB fragment (C_2AB), C_2B domain (C_2B) and SNARE complex (SC) are indicated. Note that the C_2AB fragment runs above the SNARE complex (panels A,C) but the C_2B domain runs below the SNARE complex (panels B,D) because of its smaller size. Note also that the KK and DN mutant C_2AB fragments run slightly differently than the WT C_2AB fragment, which most likely arises because the mutations change charged residues.

Table 1

Summary of apparent K_d and I_b values obtained from fitting the SNARE complex/synaptotagmin-1 fragment binding curves.

	C_2AB WT	**C_2AB DN**	**C_2AB RR**	**C_2AB KK**
K_d (μM)	2.32 ± 0.15	0.73 ± 0.33	0.94 ± 0.01	3.74 ± 1.29
I_b	0.29 ± 0.07	0.44 ± 0.01	0.48 ± 0.03	0.34 ± 0.07
	C_2B WT	C_2B RR	C_2B KK	
K_d (μM)	0.80 ± 0.39	0.40 ± 0.30	3.78 ± 1.99	
I_b	0.17 ± 0.05	0.51 ± 0.04	−0.03 ± 0.09	